

Article

Y₂O₃:Eu³⁺ Nanophosphor-Coated Mica or TiO₂/Mica as Red-Emitting Pearl Pigment: Coating Factors, Luminescent and Gloss Properties

Se-Min Ban ^{1,2,†}, Mahboob Ullah ^{1,†}, Kyeong Youl Jung ³, Byung-Ki Choi ⁴, Kwang-Jung Kang ⁴,
Myung Chang Kang ^{2,*}  and Dae-Sung Kim ^{1,*}

- ¹ A Energy & Environment Division, Korea Institute of Ceramic Engineering & Technology (KICET), Jinju 52851, Gyeongsangnam-do, Korea; bsm38@kicet.re.kr (S.-M.B.); mahboob2018@kicet.re.kr (M.U.)
² Graduate School of Convergence Science, Pusan National University, Geumjeong-gu, Pusan 46241, Korea
³ Department of Chemical Engineering, Kongju National University, Gongju 31080, Chungcheongnam-do, Korea; kyjung@kongju.ac.kr
⁴ CQV Co., 144, Seongjung-Ro, Jincheon-Eup, Jincheon-gun 27845, Chungcheongbuk-do, Korea; bkchoi@cqv.co.kr (B.-K.C.); labsmf@cqv.kr (K.-J.K.)
* Correspondence: kangmc@pusan.ac.kr (M.C.K.); dskim@kicet.re.kr (D.-S.K.);
Tel.: +82-51-510-2361 (M.C.K.); +82-55-792-2453 (D.-S.K.)
† These authors contributed equally to this work.



Citation: Ban, S.-M.; Ullah, M.; Jung, K.Y.; Choi, B.-K.; Kang, K.-J.; Kang, M.C.; Kim, D.-S. Y₂O₃:Eu³⁺ Nanophosphor-Coated Mica or TiO₂/Mica as Red-Emitting Pearl Pigment: Coating Factors, Luminescent and Gloss Properties. *Appl. Sci.* **2021**, *11*, 4365. <https://doi.org/10.3390/app11104365>

Academic Editor: Filippo Berto

Received: 12 April 2021

Accepted: 4 May 2021

Published: 11 May 2021

Publisher's Note: MDPI stays neutral with regard to jurisdictional claims in published maps and institutional affiliations.



Copyright: © 2021 by the authors. Licensee MDPI, Basel, Switzerland. This article is an open access article distributed under the terms and conditions of the Creative Commons Attribution (CC BY) license (<https://creativecommons.org/licenses/by/4.0/>).

Abstract: Red-emitted Y₂O₃:Eu³⁺ nanophosphor coated on a mica flake (Y₂O₃:Eu@MF) or on TiO₂ having a rutile crystalline mica flake (Y₂O₃:Eu@TMF) has been prepared by an electrostatic interaction with the wet-coating method for the purpose of a pigment with luminescent and gloss properties. Aggregated Y₂O₃:Eu³⁺, prepared by the template method, was dispersed into nanosol by a controlled bead-mill wet process. The (+) charged Y₂O₃:Eu³⁺ nanosol was effectively coated on the (−) charged mica flake (MF) or the TiO₂/mica flake (TMF) by an electrostatic interaction between the Y₂O₃:Eu³⁺ nanoparticles and MF or TMF at pH 6–8. The coating factors of Y₂O₃:Eu@MF were also studied and optimized by controlling the pH, stirring temperature, calcination temperature, and coating amount of Y₂O₃:Eu³⁺. The Y₂O₃:Eu³⁺ was partially coated and optimized on the MF or TMF surface with a coating coverage of about 40–50% or 60–70%, respectively. Y₂O₃:Eu@MF and Y₂O₃:Eu@TMF were exhibiting the luminescent property of a red color under a 254 nm wavelength, and had a color purity of over 95% according to CIE chromaticity coordinates. These materials were characterized by X-ray diffraction, FE-SEM, zeta potential, and a fluorescence spectrometer. These materials with luminescent and gloss properties prepared in this work potentially meet their applications for security purposes.

Keywords: red-emitted nanophosphor; Y₂O₃:Eu³⁺-coated mica or TiO₂/mica; luminescence; gloss; pearl pigment

1. Introduction

Europium-doped Y₂O₃ (Y₂O₃:Eu³⁺) is an important red phosphor, which is known for various applications due to its excellent optical properties. This kind of phosphor has been a great interest in fields such as transparent ceramics [1,2], white light-emitting diode phosphors [3], up-conversion, commercial lighting materials [3,4], plasma display panels, biomedical applications, sensors, cathode ray tubes, finger print detection [5], fluorescence sensors, medical images, illumination, and optical display technology [6]. These materials have also been used for security inks, security pigments, and biological diagnostics to prevent duplication [7]. This may be due to its luminescence properties, such as high quantum efficiency, brightness, color purity, and good absorption ability of UV radiation [8,9]. Y₂O₃:Eu³⁺ materials are being extensively studied owing to their better red emission, good thermal stability, uniformity, and better cohesion on substrate surfaces [10].

In order to obtain better luminescent properties, the phosphor materials should have a homogeneous distribution of the activator in the host matrix, with high crystallinity and phase purity [11]. Due to the aforementioned advantages, various methods have been employed for the synthesis of this material, including the sol-gel process, precipitation, hydrothermal, combustion, spray pyrolysis [12], and solid-state reaction (SSR) [10,11]. However, the products obtained by the SSR method have some disadvantages, such as non-homogeneous phase distribution, a bulky and non-uniform particle shape, which may degrade the luminescence properties of the phosphors. Such problems have been overcome by using a novel liquid-phase precursor approach or the confined space method using a template source, which may be a good way to prepare these materials with excellent luminescence properties [12,13].

Particle coating technology has applications in drug layering [14], security pigments [12], cosmetics [15], and specialty pigments. The coating ability can be controlled by employing electrostatic interaction, along with modifying the surface of particles before coating. As nanosized particles are unstable due to their high specific surface area, wet-in-wet coating is easier to be used for coating the base material surface equally in an aqueous environment. We have recently reported that lanthanide-based nanophosphor and its dispersed nanosol with good luminescent property have the potential to be applied for security purposes [16]. Mica flake coated by $\text{CeO}_2:\text{Eu}^{3+}/\text{Na}^+$ as a red phosphor was produced as a security pigment that emits red light luminescent enough to be visible to the eyes [12,17]. We have also published the $\text{Gd}_2\text{O}_3:\text{Eu}/\text{Bi}$ as a red-emitting nanophosphor coated on TiO_2/mica as a pearl pigment for security purposes [18]. Generally, the pearl pigments have a two-dimensional substrate such as the mica flake with a low refractive index and TiO_2 as a coating layer with a high refractive index. The pearl pigments are mainly used as a security material with gloss properties due to their unique sparkling and color change [18–20]. These materials are expected to be used as next-generation anti-counterfeiting pigments [12,18]. To make high luminescent pearl-type security materials, there are two ways, one is the pearl pigment should have an excellent fluorescent property and another way is to coat high luminescent nanophosphor on its surface. However, the coating of high luminescent nanophosphor is a good way to obtain a high luminescent security pigment.

$\text{Y}_2\text{O}_3:\text{Eu}^{3+}$ shows a good red emission due to the Eu^{3+} under 254 nm UV excitation. In order to achieve better luminescent characteristics, the template method is considered to be a better synthesis technique to obtain a high luminescent nanophosphor. We have hypothesized to prepare $\text{Y}_2\text{O}_3:\text{Eu}^{3+}$ by the template method and to convert it into a highly dispersed nanosol form under a controlled bead-mill wet process and to coat them on MF or TMF. The $\text{Y}_2\text{O}_3:\text{Eu}^{3+}$ is experimentally coated on MF or TMF by optimizing their coating factors, such as pH, stirring temperature, coating amount, and calcination temperature. Finally, the luminescent property of $\text{Y}_2\text{O}_3:\text{Eu}@\text{MF}$ or $\text{Y}_2\text{O}_3:\text{Eu}@\text{TMF}$ red phosphors was also investigated. However, no report has been published on preparing $\text{Y}_2\text{O}_3:\text{Eu}^{3+}$ nanosol using the bead-mill wet process, and their coating on MF or TMF. Finally, this study confirmed that $\text{Y}_2\text{O}_3:\text{Eu}^{3+}$ coated on MF or TMF can be applied for the preparation of a photo-functional security pigment with anti-counterfeiting properties.

2. Materials and Methods

2.1. Materials

In this work, all starting materials for the preparation of $\text{Y}_2\text{O}_3:\text{Eu}^{3+}$ and its nanosol were used without further purification, yttrium oxide (Samchun Chem., Seoul, Korea, 99.99%) and europium oxide (Sigma-Aldrich, Aldrich, MN, USA, 99.99%). HNO_3 (Daejung Chem., Shiheung, Korea, 60%) was used as the dissolution solvent. Distilled water was used throughout the experiments. Acrylate copolymer (BYK Co., Wesel, Germany) was used as the dispersing agent. Mica flake (MF, CQV Co., Seongjung-Ro, Korea, particle size: 9–45 μm) or TiO_2 coated on mica flake (TMF, CQV Co., Seongjung-Ro, Korea, particle size:

5–35 μm) powders were supplied from CQV Co. Especially, TMF consists of the mica flake coated and covered completely by rutile phase TiO_2 along with 50–70 nm thickness.

2.2. Preparation of $\text{Y}_2\text{O}_3:\text{Eu}^{3+}$ Coated on MF or TMF

Aggregated $\text{Y}_2\text{O}_3:\text{Eu}^{3+}$ nanoparticles were synthesized by a template method. The $\text{Y}_2\text{O}_3:\text{Eu}^{3+}$ was dispersed into nanosol by bead-mill process [21]. The size of primary particles was in the range of 85–130 nm, while the concentration of nanosol after milling was 2 wt%. $\text{Y}_2\text{O}_3:\text{Eu}@\text{MF}$ or $\text{Y}_2\text{O}_3:\text{Eu}@\text{TMF}$ were prepared by wet coating method as described below. First, 10 g MF or TMF were added in 100 mL distilled water or ethanol and stirred for 20 min at room temperature. The initial pH of the solution was adjusted to 6–8, by adding 1 M HCl or NaOH, and stirred for 20 min. $\text{Y}_2\text{O}_3:\text{Eu}^{3+}$ (50 mL) nanosol of 5–30 wt% (based on MF or TMF weight) was injected slowly with 0.2 mL/min feeding rate into the MF or TMF's slurry along with stirring at 200 rpm. Finally, the mixture was again adjusted to pH 6–8, and then treated at 65–95 $^\circ\text{C}$ for 24 h. The resultant products were filtered and washed with distilled water and dried at 100 $^\circ\text{C}$ for 4 h. The dried powders were calcined at 600–850 $^\circ\text{C}$ for 4 h to coat tightly and enhance the luminescent property. In order to optimize the coating ability of the $\text{Y}_2\text{O}_3:\text{Eu}^{3+}$ nanoparticle on the surface of MF or TMF, it was carried out by varying factors such as pH, $\text{Y}_2\text{O}_3:\text{Eu}^{3+}$ coating amount, and reaction temperature, as summarized in Table 1. While the schematic diagram for the preparation of $\text{Y}_2\text{O}_3:\text{Eu}@\text{MF}$ or $\text{Y}_2\text{O}_3:\text{Eu}@\text{TMF}$ is shown in Figure 1.

Table 1. Coating conditions of $\text{Y}_2\text{O}_3:\text{Eu}@\text{MF}$ and $\text{Y}_2\text{O}_3:\text{Eu}@\text{TMF}$ red phosphors.

Sample	Coating Condition					
	Solvent	$\text{Y}_2\text{O}_3:\text{Eu}^{3+}$ Loaded Amount Based on MF or TMF (wt%)	pH	Stirring Temperature ($^\circ\text{C}$)	Calcination Temperature ($^\circ\text{C}$)	
$\text{Y}_2\text{O}_3:\text{Eu}@\text{MF}$	Ethanol	10	7	65		
			8			
			7			
	H ₂ O	10	8	85		650
			75			
			95			
$\text{Y}_2\text{O}_3:\text{Eu}@\text{TMF}$		20	85	750		
				850		
				650		

2.3. Preparation of the Film of $\text{Y}_2\text{O}_3:\text{Eu}@\text{MF}$ and $\text{Y}_2\text{O}_3:\text{Eu}@\text{TMF}$

In order to measure gloss property, the film of $\text{Y}_2\text{O}_3:\text{Eu}@\text{MF}$ or $\text{Y}_2\text{O}_3:\text{Eu}@\text{TMF}$ was prepared as describe below. The coating slurries of two kinds of powder were respectively added in NC (nitrocellulose) resin and stirred for 1 min at 3000 rpm by a speed mixing machine. The coating slurries were uniformly painted on an opacity chart (paper film supplied from CQV Co., Korea) with 200 μm thickness.

2.4. Characterization

The crystal phase of the $\text{Y}_2\text{O}_3:\text{Eu}^{3+}$ and $\text{Y}_2\text{O}_3:\text{Eu}@\text{MF}$ was identified by X-ray diffraction (XRD, DMAX 2500, Rigaku, Wilmington, MA, USA) measurement. Particle size

distribution of $Y_2O_3:Eu^{3+}$ nanosol was observed by a particle size analyzer (PSA, ELS-Z, Otsuka Electronics, Tokushima, Japan). The zeta potential of $Y_2O_3:Eu^{3+}$, MF and TMF was analyzed by ELS-Z. To improve reliability of measurements, the average value was obtained by measuring 4 times. Field emission scanning electron microscopy (FE-SEM, JSM-6700F, JEOL, Akishima, Japan) was used to analyze the coating image and coverage of $Y_2O_3:Eu^{3+}$ particles coated on MF or TMF surface. The emission or excitation spectra of all the prepared samples were measured by spectrophotometer (LS 50, PerkinElmer, Waltham, MA, USA). The gloss properties of these films prepared with MF, TMF, $Y_2O_3:Eu@MF$, and $Y_2O_3:Eu@TMF$ were measured using a micro-TRI-gloss meter (BYK Gardner, Wesel, Germany). In this case, a glass plate with a refractive index of 1.567 was used as the standard sample. Gloss was measured by projecting a beam of light at 20° , 60° , and 85° angles onto the film surface.

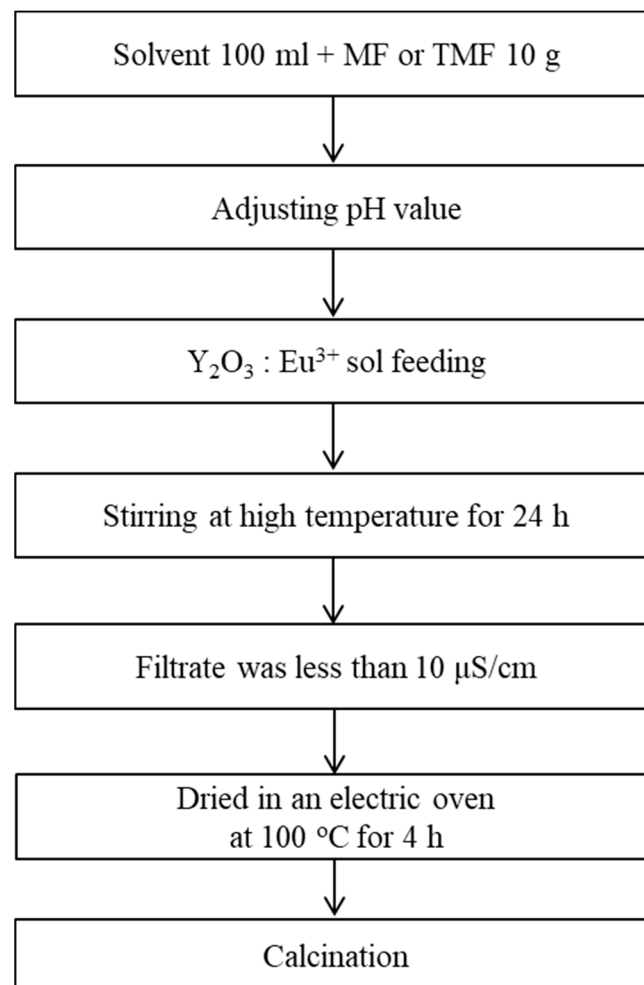


Figure 1. Preparation process of $Y_2O_3:Eu^{3+}$ red phosphor coated on MF or TMF.

3. Results

3.1. $Y_2O_3:Eu@MF$ Prepared by the Variation in pH and Solvents

To disperse the aggregated $Y_2O_3:Eu^{3+}$ nanophosphor prepared by the template method, the $Y_2O_3:Eu^{3+}$ nanosol was prepared and optimized by controlling the solvents, pH, and a dispersant agent (acrylate copolymer) to improve the dispersibility under the bead-mill wet process.

Figure 2 displays the particle size distribution of the $Y_2O_3:Eu^{3+}$ nanosol dispersed in ethanol or water. The nanosol dispersed in ethanol, as in Figure 2a, has around 134 nm of the median particle size (D_{50}), whereas that in water, Figure 2b, has around 120 nm [21].

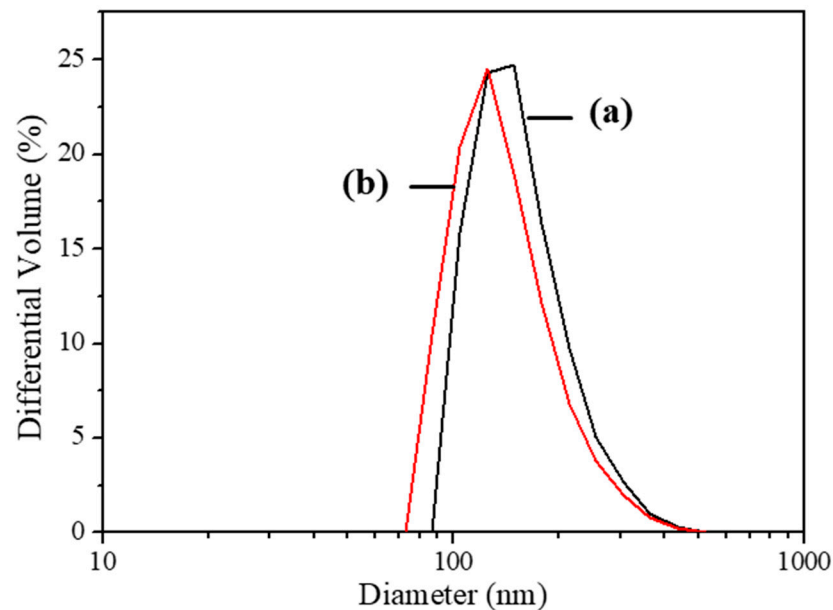


Figure 2. Median particle size (D_{50}) of $Y_2O_3:Eu^{3+}$ nanosol dispersed in (a) ethanol and (b) H_2O as solvent.

Here, the zeta potential of the $Y_2O_3:Eu^{3+}$ dispersed in H_2O is 40.4 mV, but 15.3 mV in ethanol. Generally, if the absolute value of the zeta potential is more than 30 mV, the dispersion stability is excellent due to the strong repulsive force between the particles [22]. It can be explained that the $Y_2O_3:Eu^{3+}$ dispersed in H_2O is more stable than that dispersed in ethanol. Also, H_2O and ethanol are both hydrophilic. The difference of the dispersions in the two solutions is considered to be the relative polarity. While H_2O has only a hydroxyl group which is hydrophilic, ethanol has a hydroxyl group and an alkyl group, which is lipophilic [23], so the difference in polarities is expected to have caused a difference in the dispersion stability.

To coat $Y_2O_3:Eu^{3+}$ nanoparticles on the surface of the mica flake (MF), the electrostatic attraction between the two particles was observed via the zeta potential of $Y_2O_3:Eu^{3+}$ and MF. Figure 3 shows the zeta potential curves of the MF and $Y_2O_3:Eu^{3+}$ particles measured in the pH range of 1–10. In the case of MF, the zeta potential tends to decrease from +30 mV to −55 mV on increasing the pH from 1 to 10. The isoelectric point (IEP) of mica is at about a pH of 5.5. $Y_2O_3:Eu^{3+}$ nanoparticles modified with an acrylic copolymer have a (+) charge in the entire pH range. Therefore, the coating process between $Y_2O_3:Eu^{3+}$ and mica is considered to be the most effective in the pH range of 7–9, at which the potential difference is the highest.

Figure 4 displays the FE-SEM images of the $Y_2O_3:Eu@MF$ red phosphors prepared by varying the pH of ethanol or water. Figure 4a,b show the surface of the $Y_2O_3:Eu@MF$ at pH 7 and 8, respectively, in the ethanol system. It was confirmed that the coating coverage ratio of the $Y_2O_3:Eu^{3+}$ particles on the surface of MF was about 5% or less. The sample prepared at pH 7 in the water system was about 1–5%, as depicted in Figure 4c. Interestingly, the sample prepared at pH 8 was coated with 30–40% coverage of $Y_2O_3:Eu^{3+}$, as shown in Figure 4d. Under the condition of pH 8, the zeta potential difference between the surface charge of the (+) charged $Y_2O_3:Eu^{3+}$ and the (−) charged mica was 85 mV. It means that the two particles interact more effectively and are coated to prepare $Y_2O_3:Eu@MF$. Therefore, $Y_2O_3:Eu@MF$ was carried out at pH 8 in the water environment in order to optimize the coating ability of the $Y_2O_3:Eu^{3+}$ nanoparticles.

Figure 5 shows the XRD patterns of MF and $Y_2O_3:Eu@MF$. MF was observed to be well crystallized, belonging to a phlogopite (JCPDS No. 16-0344) as depicted in Figure 5a,b shows that the enlarged XRD pattern of $Y_2O_3:Eu@MF$ (10 wt%) is matched well with the cubic structure of Y_2O_3 (JCPDS No. 76-0151) along with a phlogopite Mica structure.

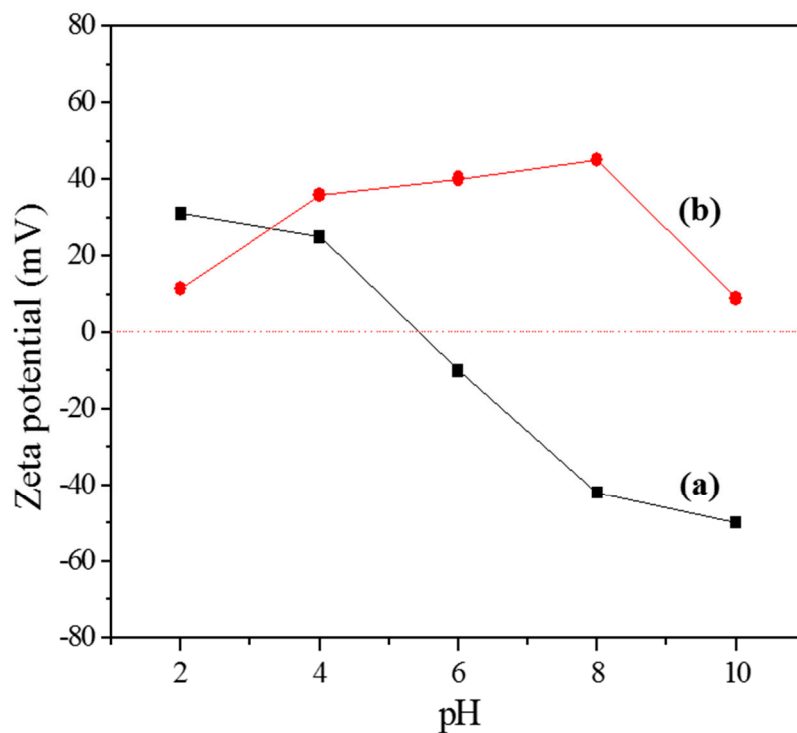


Figure 3. Zeta potential curves of (a) mica and (b) $Y_2O_3:Eu^{3+}$ as a function of pH.

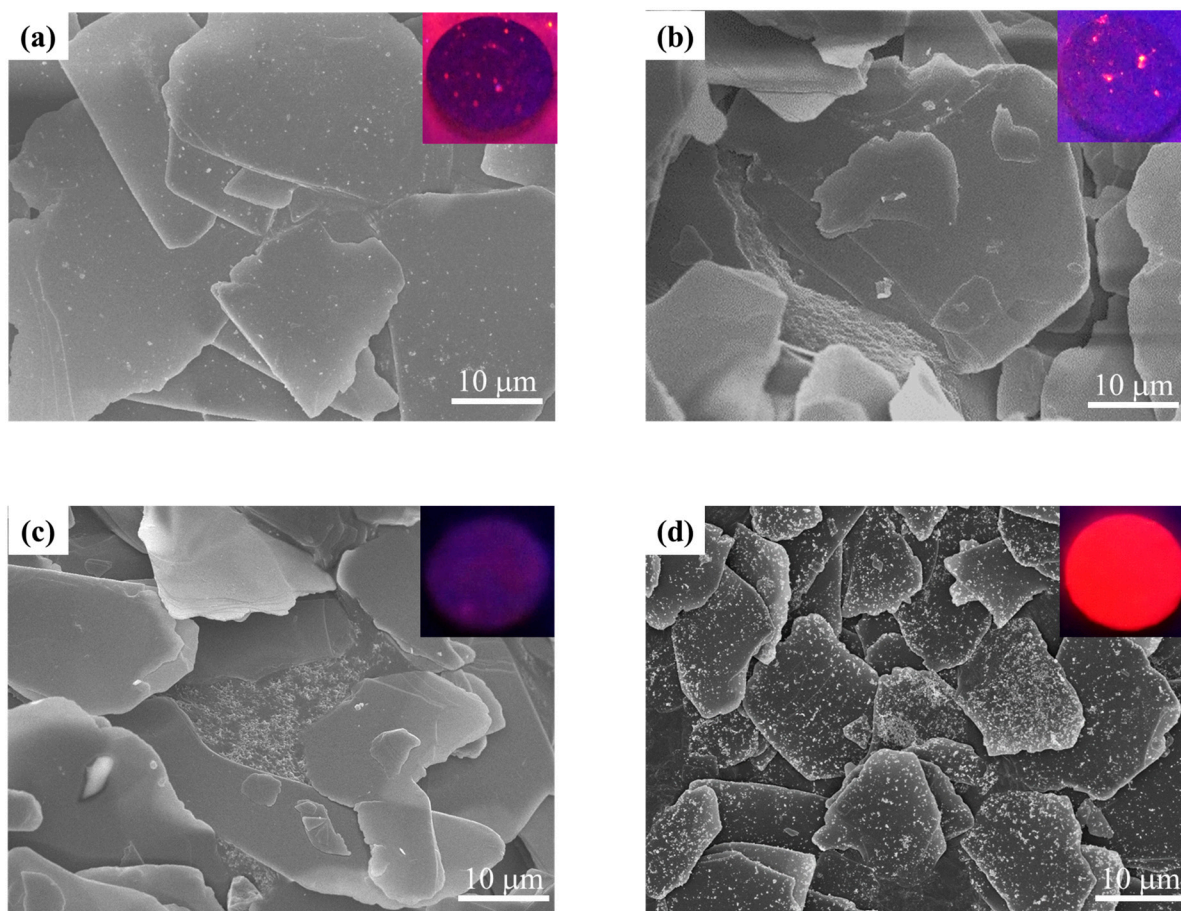


Figure 4. FE-SEM images and inserted fluorescent pictures, of the powders exposed under UV lamp, of $Y_2O_3:Eu@MF$ calcined at $650\text{ }^\circ\text{C}$ after coating at (a) pH 7 and (b) pH 8 in ethanol, (c) pH 7, and (d) pH 8 in water.

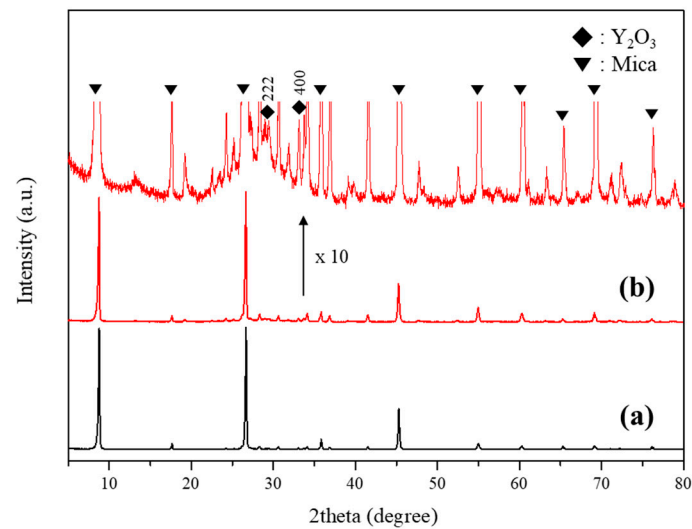


Figure 5. Powder XRD patterns of (a) mica flake and (b) $\text{Y}_2\text{O}_3:\text{Eu@MF}$ (10 wt%).

Figure 6 shows the photoluminescence (PL) spectra of the $\text{Y}_2\text{O}_3:\text{Eu@MF}$ red phosphor prepared by the variation in the calcination temperature at pH 7 in ethanol and pH 8 in water. The PL measurement range was 400–800 nm and the emission spectrum was fixed and measured at the center wavelength of 254 nm as it is the dominant excitation peak. The emission spectra peak appeared at 560 nm to 635 nm, and the weak peak was also observed at 710 nm. The relative transition of various emission spectra was due to the transition of $^5\text{D}_0 \rightarrow ^7\text{F}_j$ ($J = 0-4$) in relation to the Eu^{3+} ions. The most intense peak at 611 nm, depicted in Figure 6, could be identified as the transition from the splitting level of $^5\text{D}_0 \rightarrow ^7\text{F}_2$ of the Eu^{3+} ions [24]. As shown in Figure 6a, the emitted red light was very weak and dark. On the other hand, a bright red emission is shown in the inserted photograph in Figure 6b. As a result, the luminescent intensity of $\text{Y}_2\text{O}_3:\text{Eu@MF}$, prepared with pH 8 in H_2O , was higher than that of the sample prepared in ethanol.

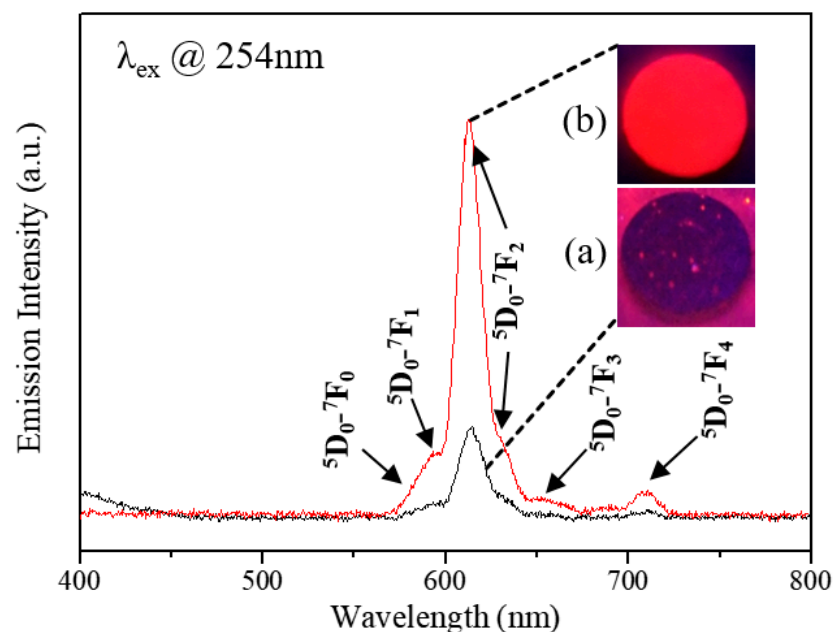


Figure 6. Photoluminescence spectra of $\text{Y}_2\text{O}_3:\text{Eu@mica}$ red phosphor calcined at 650°C after coating at (a) pH 7 in ethanol, and (b) at pH 8 in water.

3.2. $Y_2O_3:Eu@MF$ Prepared by Varying Coating Amount of $Y_2O_3:Eu^{3+}$ and Temperatures

The $Y_2O_3:Eu@MF$ was finally prepared and optimized by varying the loading amount of $Y_2O_3:Eu^{3+}$, stirring temperature, and calcination temperature.

Figure 7 shows the FE-SEM images of $Y_2O_3:Eu@MF$ prepared by 5, 10, and 20 wt% coatings of $Y_2O_3:Eu^{3+}$ nanoparticles on mica in water. It can be seen that the $Y_2O_3:Eu^{3+}$ nanoparticles having size less than 100 nm were individually coated on the mica flake (MF, 9–45 μm in size). As the coating amount of the nanoparticles was 5 wt% as shown in Figure 7a, the coating coverage of $Y_2O_3:Eu@MF$ was about 10–20%. The coating coverage was calculated as the ratio of the coated nanoparticles area to the mica surface by the average value after manually mapping several sample images. The coating coverage has been increased with the increasing loading amount of the nanoparticles, as shown in Figure 7b. Herein, the coating coverage of $Y_2O_3:Eu@MF$ (10 wt%) was about 40–50%. However, as the loading amount exceeded 10 wt%, the coating coverage of the nanoparticles on mica decreased because of the aggregation of the nanoparticles.

In order to investigate the coating property and ability of the stirring and calcination temperatures, $Y_2O_3:Eu@MF$ was fixed and prepared at pH 8 as depicted in Figures 8 and 9.

Figure 8 shows the FE-SEM images of the $Y_2O_3:Eu@MF$ prepared with a 20 wt% loading amount of $Y_2O_3:Eu^{3+}$ at stirring temperatures of 75, 85, and 95 $^{\circ}C$, respectively. As the temperature increased, it was confirmed that the $Y_2O_3:Eu^{3+}$ nanoparticles are effectively coated on the surface of MF. After the coating reaction completed in the initial solution at pH 8, the final pH of the resultant solution was slightly higher than pH 8 at 85 $^{\circ}C$ and 95 $^{\circ}C$, but was slightly lower than pH 8 at 75 $^{\circ}C$. As can be seen from the zeta potential curve in Figure 3, that the potential difference is larger and the coating property is better at pH 8. As the temperature increases, the ions in the solution move actively; this affects its pH. It is considered that the attractive force of the $Y_2O_3:Eu^{3+}$ nanoparticles is strengthened as they get coated on the surface of MF. Especially, the results with a stirring temperature of 95 $^{\circ}C$ are not significantly different from those of 85 $^{\circ}C$; the stirring temperature at 85 $^{\circ}C$ was considered to be the most suitable.

Figure 9 shows the FE-SEM images of the obtained $Y_2O_3:Eu@MF$ for different calcination temperatures. Figure 9a clearly shows that the $Y_2O_3:Eu@MF$ calcined at 650 $^{\circ}C$ is stably attached on the mica surface. Compared to the samples calcined at 750 $^{\circ}C$, Figure 9b, and 850 $^{\circ}C$, Figure 9c, it was found that the $Y_2O_3:Eu^{3+}$ nanoparticles were detached from the mica surface. This phenomenon occurs due to the different thermal expansions of the $Y_2O_3:Eu^{3+}$ nanoparticles and mica.

Figure 10 depicts the PL emission spectra fixed at 254 nm excitation of the $Y_2O_3:Eu@MF$ powders as red phosphor shown in Figure 9. The emission intensity of the sample calcined at 650 $^{\circ}C$ was higher than that of the two samples calcined at 750 $^{\circ}C$ or 850 $^{\circ}C$. The brightness of these red-emitted phosphors in the images inserted in Figure 9 is decreased accordingly with the increase in the calcination temperature. This result was considered to be proportional to the coating coverage or the number of $Y_2O_3:Eu^{3+}$ nanoparticles coated on mica, and to be detached due to the difference in the coefficient of the thermal expansion between the $Y_2O_3:Eu^{3+}$ and mica particles according to the increase in the temperature, as shown in Figure 9. Also, it was confirmed that the luminescent property of the nanoparticles with low crystallinity, caused by milling, increased with the increasing crystallinity of the coated nanoparticles after the calcination process of $Y_2O_3:Eu@MF$. Kim group had reported that the luminescent property of $Y_2O_3:Eu^{3+}$ nanoparticles was recovered after the calcination process in spite of the decreased crystal structure of the nanoparticles due to the bead-mill process [21].

Figure 11a shows the cross-sectional FE-SEM image of the $Y_2O_3:Eu@MF$ (10 wt%) particle, fixed in epoxy resin, captured to observe the coating thickness. The powder was mixed with epoxy resin and then dried and prepared to measure its coating thickness. Based on the FE-SEM image, it has been concluded that the MF coated with the $Y_2O_3:Eu^{3+}$ nanoparticle was surrounded by epoxy resin. Herein, the bright plate of the top and bottom layer indicates epoxy resin and the dark middle layer consists of MF. The mica flake of

the middle layer was coated by $\text{Y}_2\text{O}_3:\text{Eu}^{3+}$ nanoparticles of the bright part. However, the coated nanoparticles on MF were observed only on the bottom side due to the covered epoxy plate on the top side. The thickness range of the mica and $\text{Y}_2\text{O}_3:\text{Eu}^{3+}$ nanoparticles was about 284 nm, and 80–105 nm, respectively. Multi-elemental EDS mapping images of Y, Si, and Ti are shown in Figure 11a. Apparently, the corresponding Y and Si maps evidenced bright spots corresponding to the $\text{Y}_2\text{O}_3:\text{Eu}$ red phosphor and mica area, and illustrated the coating layers of these elements in the field of view of the cross-section.

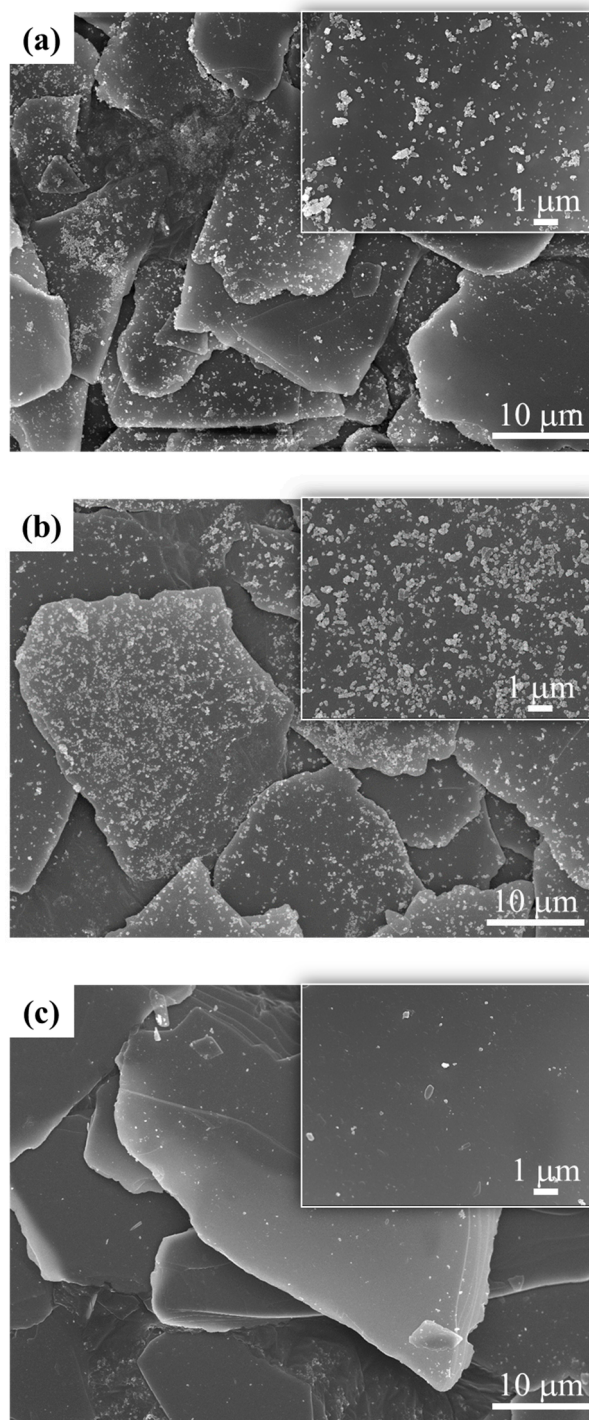


Figure 7. FE-SEM images of $\text{Y}_2\text{O}_3:\text{Eu}^{3+}@\text{MF}$ prepared by the variation in $\text{Y}_2\text{O}_3:\text{Eu}^{3+}$ loading amount, (a) 5 wt%; (b) 10 wt%; and (c) 20 wt% (fixed at pH 8 under 85 °C in H_2O).

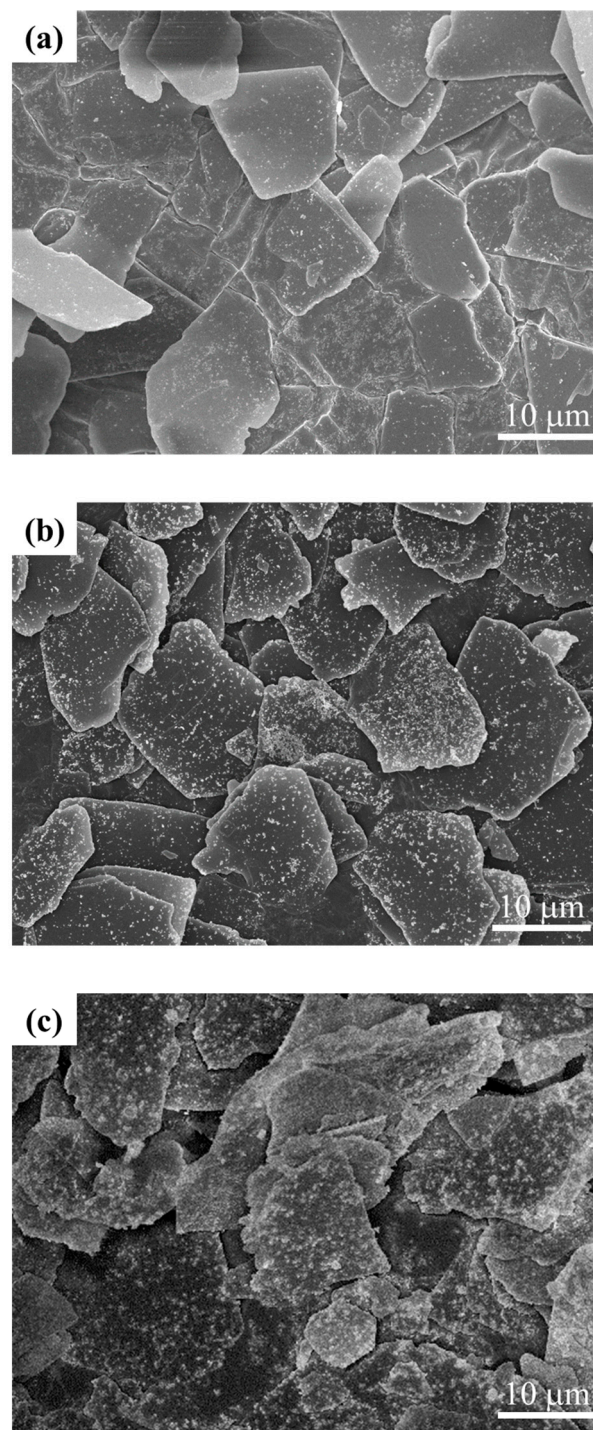


Figure 8. FE-SEM images of $\text{Y}_2\text{O}_3:\text{Eu@MF}$ prepared by the variation in stirring temperature, (a) 75 °C; (b) 85 °C; and (c) 95 °C (fixed at pH 8 in H_2O and $\text{Y}_2\text{O}_3:\text{Eu}^{3+}$ loading amount 20 wt%).

Figure 11b shows the cross-sectional FE-SEM image of the $\text{Y}_2\text{O}_3:\text{Eu@TMF}$ (20 wt%) particle. The particle consists of the following three layers: the middle layer is the mica flake (MF) having about 314 nm thickness, and the TiO_2 layers coated on the MF have about 58 nm thickness, while the outside layers (bright part) coated on TMF are coated with Y_2O_3 having about 162 nm thickness. For the MF or TMF information, these materials show different thicknesses (300–800 nm) depending on the observing spot. To identify the elements of coating layers, EDS mapping images of Y, Si, and Ti are shown in Figure 11b. The Si element of the mica layer and the Y element of the $\text{Y}_2\text{O}_3:\text{Eu}^{3+}$ red phosphor layer

were clearly identified, as compared to Figure 11a. The Ti element of the TiO_2 layer coated on mica (TMF) is also clearly visible between the mica and the red phosphor layers. Therefore, it is demonstrated that the $\text{Y}_2\text{O}_3:\text{Eu}^{3+}$ particles were coated on the TMF particles, as shown in Figures 11b and 12b.

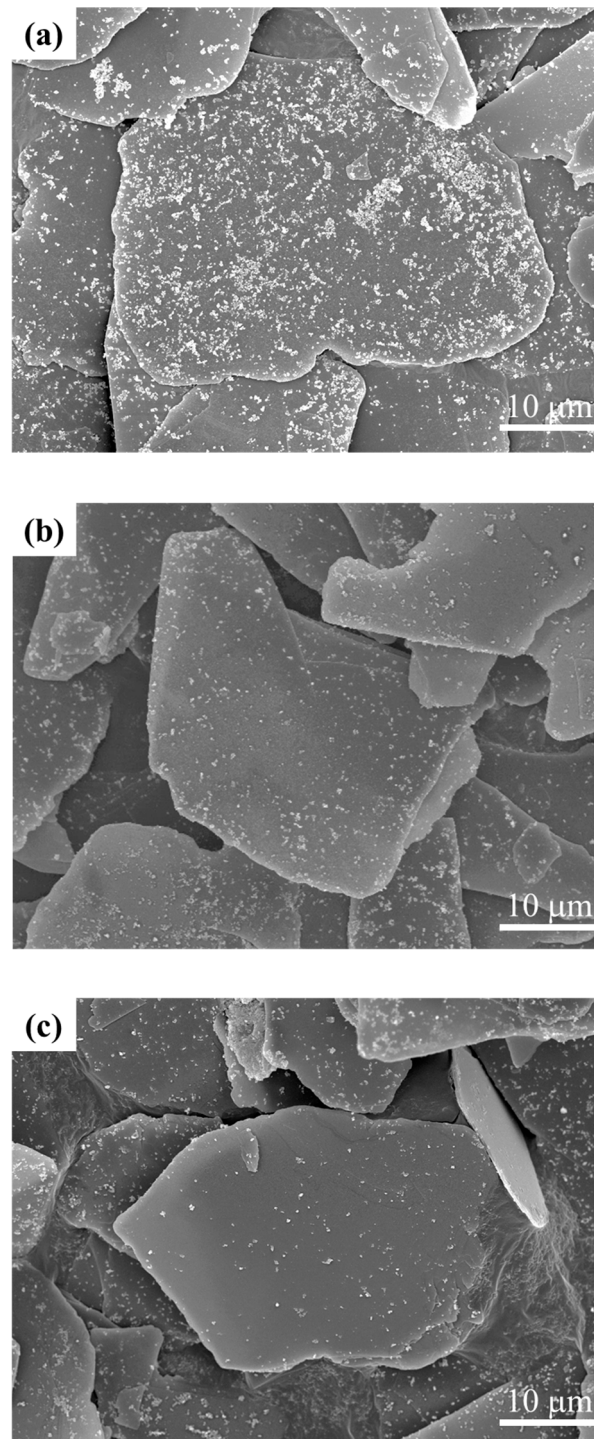


Figure 9. FE-SEM images of $\text{Y}_2\text{O}_3:\text{Eu@MF}$ prepared at the following calcination temperatures: (a) 650 °C, (b) 750 °C, and (c) 850 °C, with the synthetic condition in Figure 8b.

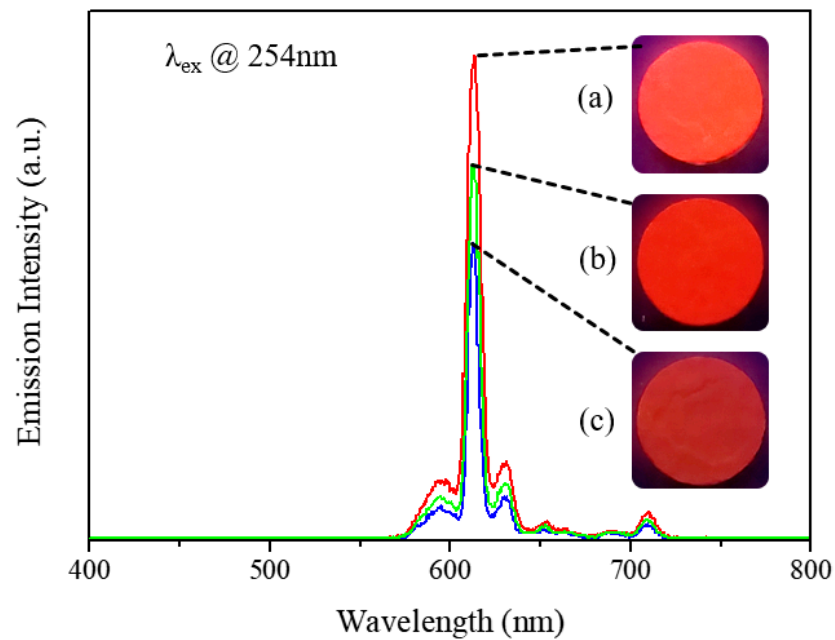


Figure 10. Photoluminescence spectra of $\text{Y}_2\text{O}_3:\text{Eu@MF}$ red phosphor calcined at (a) 650 °C, (b) 750 °C, and (c) 850 °C in Figure 9.

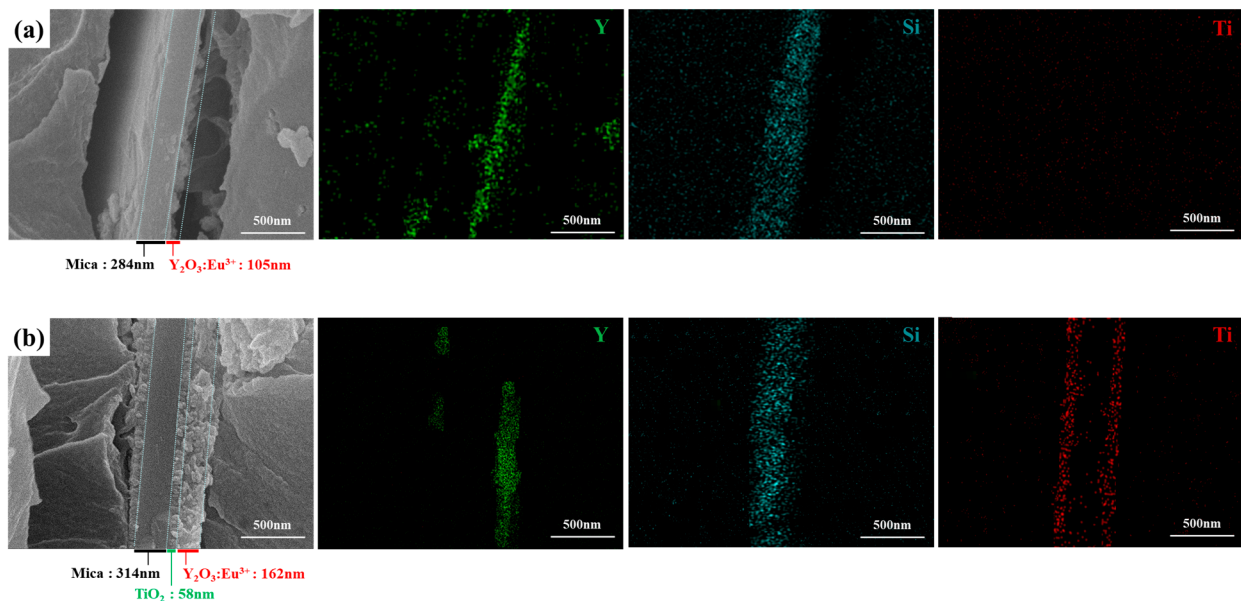


Figure 11. Cross-section FE-SEM images and EDS mapping of Y, Si and Ti elements in (a) $\text{Y}_2\text{O}_3:\text{Eu@MF}$ (10 wt%) and (b) $\text{Y}_2\text{O}_3:\text{Eu@TMF}$ (20 wt%).

3.3. Preparation of $\text{Y}_2\text{O}_3:\text{Eu@TMF}$ by Varying Loading Amount of $\text{Y}_2\text{O}_3:\text{Eu}^{3+}$

TMF is a two-dimensional material that consists of a mica flake (MF) coated completely with TiO_2 nanoparticles having a high refractive index. The pearl property of TMF can be controlled by the TiO_2 coating layers. However, we required further experiments with $\text{Y}_2\text{O}_3:\text{Eu}^{3+}$ loading amounts due to the wavelength overlaps between the UV absorption of TiO_2 and the excitation of $\text{Y}_2\text{O}_3:\text{Eu}^{3+}$ red phosphor [25].

Figure 12 shows the FE-SEM images of the $\text{Y}_2\text{O}_3:\text{Eu@TMF}$ prepared by varying the $\text{Y}_2\text{O}_3:\text{Eu}^{3+}$ loading amount from (a) 10, (b) 20, and (c) 30 wt%. In Figure 12a, the coating coverage of $\text{Y}_2\text{O}_3:\text{Eu@TMF}$ (10 wt%) was about 10–30 %. The coating coverage of $\text{Y}_2\text{O}_3:\text{Eu@MF}$ (20 wt%) in Figure 12b was about 60–70 %. Herein, the FE-SEM results

confirm that the nanoparticles are effectively coated. However, the coating coverage was rapidly decreased at the 30 wt% loading amount of $\text{Y}_2\text{O}_3:\text{Eu}^{3+}$ nanoparticles, and the agglomerated nanoparticles separated from TMF were observed as shown in Figure 12c. The cohesive ability between the $\text{Y}_2\text{O}_3:\text{Eu}^{3+}$ nanoparticles are superior than that between the nanoparticles and TMF over 20 wt% loading.

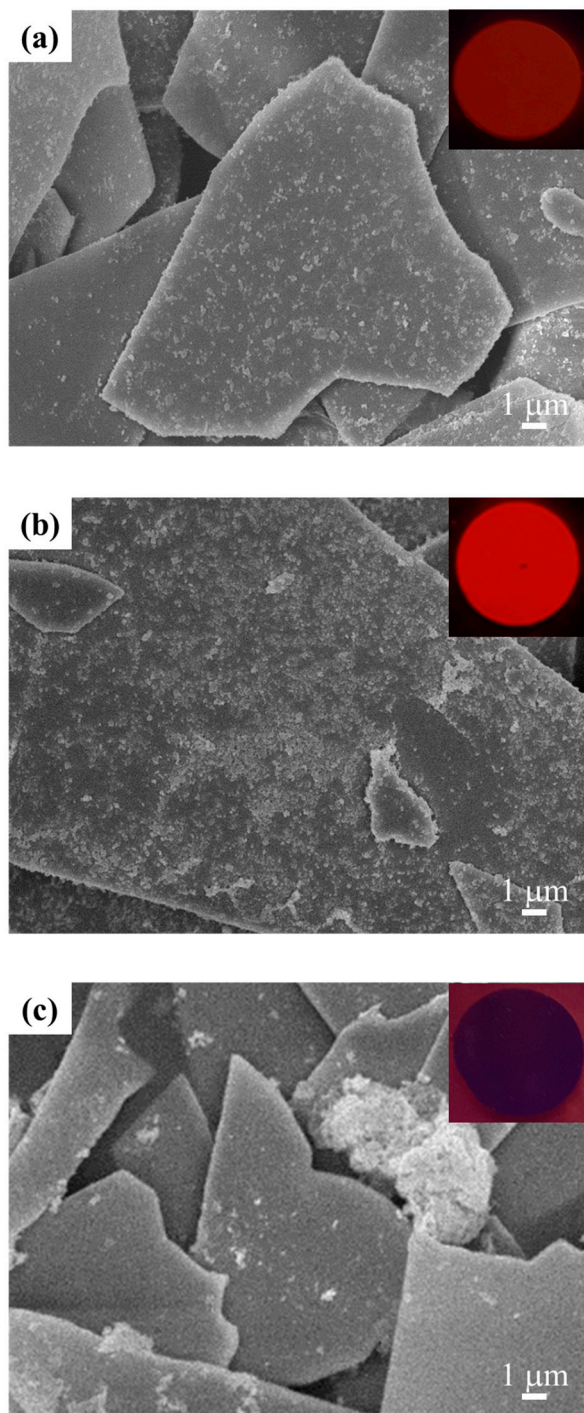


Figure 12. FE-SEM images and inserted fluorescent pictures, of the powders exposed under UV lamp, of $\text{Y}_2\text{O}_3:\text{Eu}@\text{TMF}$ prepared by the variation in $\text{Y}_2\text{O}_3:\text{Eu}^{3+}$ loading amount (a) 10 wt%, (b) 20 wt%, and (c) 30 wt% (fixed at pH 8 and 85 °C in H_2O).

3.4. Gloss and Luminescent Properties of Security Pigment Films

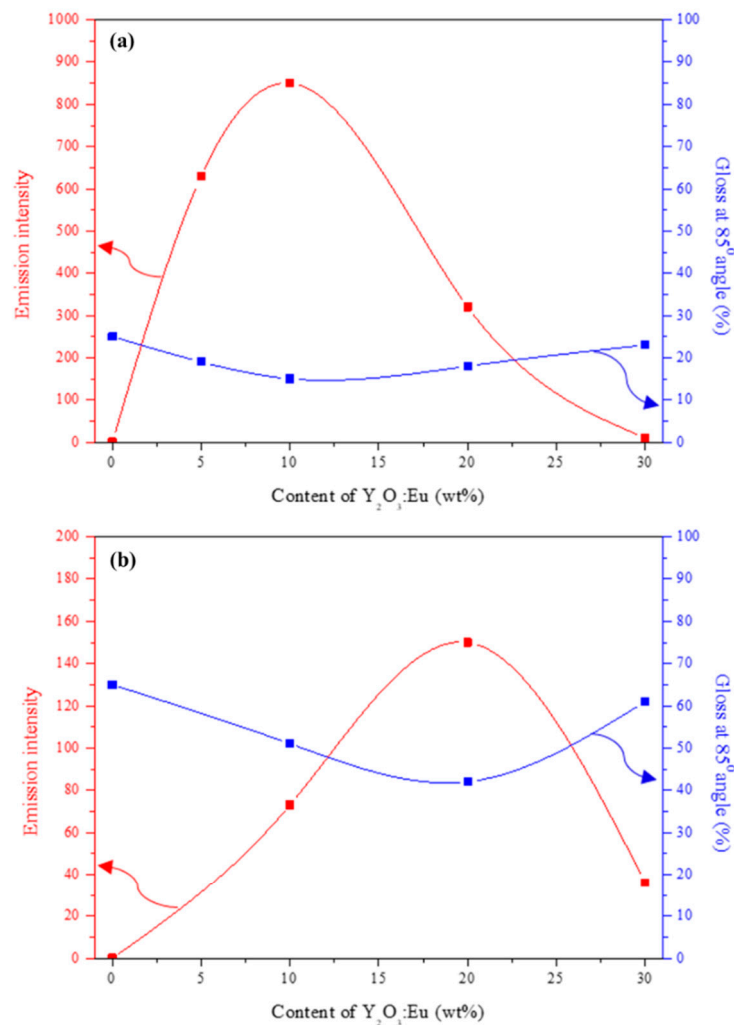
We measured the gloss characteristics of the films, which contain MF, TMF, $Y_2O_3:Eu@MF$ and $Y_2O_3:Eu@TMF$ pigments, mixed with epoxy resin to observe their correlation with luminescent properties. Table 2 shows the gloss characteristics of $Y_2O_3:Eu@MF$ and $Y_2O_3:Eu@TMF$. The gloss characteristics of TMF were higher at each angle than MF alone, which is believed to have a greater effect on TiO_2 . In addition, as the coating coverage of $Y_2O_3:Eu^{3+}$ increases, the gloss characteristic decreases, which is thought to be the effect of $Y_2O_3:Eu^{3+}$, which has a weak gloss characteristic due to the scattering of the coated particles.

Table 2. Gloss values according to the variation in angle for the film prepared by MF, TMF, $Y_2O_3:Eu@MF$ and $Y_2O_3:Eu@TMF$ security pigments.

Sample *	Gross of Angle		
	20°	60°	85°
MF	4.8	17.1	19.3
$Y_2O_3:Eu@MF$	10 wt% **	3.9	14.8
	20 wt%	4.5	16.3
TMF	17.8	58.3	62.9
$Y_2O_3:Eu@TMF$	10 wt%	14.2	42.6
	20 wt%	10.1	35.7
	30 wt%	15.3	55.1

* Film prepared by mixing sample and resin. ** $Y_2O_3:Eu^{3+}$ loading amount on MF or TMF.

Figure 13a,b display the correlation between the gloss values (85° angle) and the luminescent characteristics (λ_{em}^{max} around 611 nm) of a security pigment according to the variation in $Y_2O_3:Eu^{3+}$ amount loaded on MF or TMF. The luminescent property of $Y_2O_3:Eu@MF$ was overall better than that of $Y_2O_3:Eu@TMF$ due to the absorption UV of the TiO_2 layer coated on the MF surface. However, the gloss property of $Y_2O_3:Eu@TMF$, by TMF having the high reflective layer of TiO_2 coated on MF, was higher compared with that of $Y_2O_3:Eu@MF$. Therefore, we studied to enhance the security level along with optimizing the gloss and luminescent property of $Y_2O_3:Eu@TMF$, which was prepared at $Y_2O_3:Eu^{3+}$ loading amounts in the range of 15–25 wt%. Figure 13c shows the “KICET” mark printed on a black opacity chart using $Y_2O_3:Eu@MF$ or $Y_2O_3:Eu@TMF$ mixed with epoxy resin. One remarkable difference was observed in the mark under natural light. In the natural light, it is found that the gloss properties were stronger on the surface of $Y_2O_3:Eu@TMF$ than on $Y_2O_3:Eu@MF$. On the other hand, the mark showed a red color under the portable UV lamp ($\lambda_{em} = 254$ nm), and its red luminescent became greater for $Y_2O_3:Eu@MF$ than $Y_2O_3:Eu@TMF$. Given this, it is confirmed that the relation between the gloss and luminescent is coincident with Figure 13a,b and the mark is possible for the application as a security pigment with multi-function.



(c)	$Y_2O_3:Eu@MF$	$Y_2O_3:Eu@TMF$
Under natural light		
Under the 254nm portable UV lamp		

Figure 13. Graph of relationship between gloss at 85° angle and luminescent property of (a) $Y_2O_3:Eu@MF$ and (b) $Y_2O_3:Eu@TMF$, and (c) optical image of the “KICET” mark prepared pearl pigments mixed with epoxy resin under natural light and 254 nm portable UV lamp.

4. Conclusions

A mica flake (MF) coated with nanosized $Y_2O_3:Eu^{3+}$ ($Y_2O_3:Eu@MF$) as a red nanophosphor, was prepared by electrostatic interaction of the particles under hydrothermal conditions. $Y_2O_3:Eu@MF$ was prepared and optimized by varying the solvent, pH, stirring temperature, calcination temperature, and the loading amount of $Y_2O_3:Eu^{3+}$. The optimized condition for $Y_2O_3:Eu@MF$ was an 85 °C stirring temperature, pH 8, 10 wt% of loading amount of the $Y_2O_3:Eu^{3+}$ nanoparticle, and a 650 °C calcination temperature. In particular, when the loading amount exceeded 10 wt%, the number of nanoparticles coated on MF was reduced. The reason is due to the aggregation of the nanoparticles rather than the interaction and deposition on the surface of MF. The $Y_2O_3:Eu@MF$ calcined at

650 °C was also stably attached on the mica surface. It was confirmed that the luminescent property of the nanoparticle with low crystallinity caused by milling was recovered by increasing the crystallinity of the coated nanoparticles after the calcination process of $\text{Y}_2\text{O}_3:\text{Eu}@\text{MF}$. In the case of $\text{Y}_2\text{O}_3:\text{Eu}@\text{TMF}$, the material prepared at 20 wt% loading amount of the $\text{Y}_2\text{O}_3:\text{Eu}^{3+}$ nanoparticle had the highest coating coverage and was optimized. The photoluminescence spectra revealed the strongest emission peak centered at 611 nm is due to movement of the Eu^{3+} ions from the ${}^5\text{D}_0 \rightarrow {}^7\text{F}_2$. In cross-sectional images of FE-SEM, the thickness of the $\text{Y}_2\text{O}_3:\text{Eu}^{3+}$ particles coated on MF or TMF was around 120–270 nm. As a security pigment, the luminescent property of the $\text{Y}_2\text{O}_3:\text{Eu}@\text{MF}$ film was better overall than that of $\text{Y}_2\text{O}_3:\text{Eu}@\text{TMF}$ due to the absorption UV of the TiO_2 layer coated on the MF surface. However, the gloss property of the $\text{Y}_2\text{O}_3:\text{Eu}@\text{TMF}$ film, by TMF having the high reflective layer of TiO_2 coated on MF, was higher compared with that of $\text{Y}_2\text{O}_3:\text{Eu}@\text{MF}$. Especially, to improve the security level, the $\text{Y}_2\text{O}_3:\text{Eu}@\text{TMF}$ (20 wt%) film was prepared and optimized with red phosphor materials (having luminescent property) and pearl materials (having gloss property). Therefore, these materials with luminescent and gloss properties prepared in this work potentially meet their applications for security purposes.

Author Contributions: S.-M.B. and M.U. processed the experimental data, performed the analysis. S.-M.B. wrote the manuscript with support from M.C.K., M.U. and D.-S.K., K.Y.J. and K.-J.K. contributed to sample preparation. K.Y.J. performed the measurements and analyzed the spectra. B.-K.C. and D.-S.K. helped supervise the project. B.-K.C. and K.-J.K. conceived the original idea. All authors provided critical feedback and helped shape the research, analysis and manuscript. All authors have read and agreed to the published version of the manuscript.

Funding: This research received no external funding.

Acknowledgments: This work was supported by the Research Fund of Advanced Technology Center (ATC) Project (Project no. 10052088) at Ministry of Trade, Industry and Energy (MOTIE).

Conflicts of Interest: The authors declare no conflict of interest.

References

1. Wang, C.-N.; Li, Y.; Zhang, W.-P.; Yin, M. Effect of acidity on microstructure and spectroscopic properties of $\text{Y}_2\text{O}_3:\text{Eu}^{3+}$ powders and ceramics. *Spectrochim. Acta Part A Mol. Biomol. Spectrosc.* **2010**, *75*, 8–13. [[CrossRef](#)] [[PubMed](#)]
2. Kumar, Y.; Pal, M.; Herrera, M.; Mathew, X. Effect of Eu ion incorporation on the emission behavior of Y_2O_3 nanophosphors: A detailed study of structural and optical properties. *Opt. Mater.* **2016**, *60*, 159–168. [[CrossRef](#)]
3. Qin, X.; Zhou, G.; Yang, H.; Yang, Y.; Zhang, J.; Wang, S. Synthesis and upconversion luminescence of monodispersed, submicron-sized $\text{Er}^{3+}:\text{Y}_2\text{O}_3$ spherical phosphors. *J. Alloys Compd.* **2010**, *493*, 672–677. [[CrossRef](#)]
4. Liang, H.; Zheng, Y.; Chen, G.; Wu, L.; Zhang, Z.; Cao, W. Enhancement of upconversion luminescence of $\text{Y}_2\text{O}_3:\text{Er}^{3+}$ nanocrystals by codoping $\text{Li}^+-\text{Zn}^{2+}$. *J. Alloys Compd.* **2011**, *509*, 409–413. [[CrossRef](#)]
5. Raju, G.S.R.; Pavitra, E.; Nagaraju, G.; Yu, J.S. Versatile properties of $\text{CaGd}_2\text{ZnO}_5:\text{Eu}^{3+}$ nanophosphor: Its compatibility for lighting and optical display applications. *J. Dalton Trans.* **2015**, 1790–1799. [[CrossRef](#)]
6. Rakov, N.B.; Lozano, W.; Maciel, G.S.; De Araújo, C.B. Nonlinear luminescence in Eu^{3+} -doped Y_2O_3 powders pumped at 355 nm. *Chem. Phys. Lett.* **2006**, *428*, 134–137. [[CrossRef](#)]
7. Venkatachalaiah, K.N.; Nagabhushana, H.; Darshan, G.P.; Basavaraj, R.B.; Prasad, B.D. Novel and highly efficient red luminescent sensor based $\text{SiO}_2/\text{Y}_2\text{O}_3:\text{Eu}^{3+}$, M^+ ($\text{M}^+ = \text{Li}, \text{Na}, \text{K}$) composite core-shell fluorescent markers for latent fingerprint recognition, security ink and solid-state lightning applications. *J. Sens. Actuator B-Chem.* **2017**, *310*–325. [[CrossRef](#)]
8. Khachatourian, A.M.; Golestani-Fard, F.; Sarpoolaky, H.; Vogt, C.; Vasileva, E.; Mensi, M.; Popov, S.; Toprak, M.S. Microwave synthesis of $\text{Y}_2\text{O}_3:\text{Eu}^{3+}$ nanophosphors: A study on the influence of dopant concentration and calcination temperature on structural and photoluminescence properties. *J. Lumin.* **2016**, *169*, 1–8. [[CrossRef](#)]
9. Li, Q.; Yuan, Y.; Chen, Z.; Jin, X.; Wei, T.-H.; Li, Y.; Qin, Y.; Sun, W. Core-Shell Nanophosphor Architecture: Toward Efficient Energy Transport in Inorganic/Organic Hybrid Solar Cells. *ACS Appl. Mater. Interfaces* **2014**, *6*, 12798–12807. [[CrossRef](#)]
10. Ye, J.; Hongpeng, Z.; Dingfei, Z. Luminescence Properties of Eu/Tb Activated Y_2O_3 Phosphors Synthesized by Solid State Process. *Rare Met. Mater. Eng.* **2016**, *45*, 2790–2792. [[CrossRef](#)]
11. Zambare, A.P.; Murthy, K.V.R. Photoluminescence studies of Eu doped Yttrium based phosphors. *Arch. Phy. Res.* **2011**, *2*, 46–50.
12. Jung, K.Y.; Lee, J.C.; Kim, D.S.; Choi, B.-K.; Kang, W.-J. Co-doping effect of monovalent alkali metals on optical properties of $\text{CeO}_2:\text{Eu}$ nanophosphor prepared by spray pyrolysis and application for preparing pearlescent pigments with red emission. *J. Lumin.* **2017**, *192*, 1313–1321. [[CrossRef](#)]

13. Fisher, M.J.; Wang, W.; Dorhout, P.K.; Fisher, E.R. Synthesis of LaPO₄:Eu Nanostructures Using the Sol–Gel Template Method. *J. Phys. Chem. C* **2008**, *112*, 1901–1907. [[CrossRef](#)]
14. Win, K.Y.; Feng, S.-S. Effects of particle size and surface coating on cellular uptake of polymeric nanoparticles for oral delivery of anticancer drugs. *Biomaterials* **2005**, *26*, 2713–2722. [[CrossRef](#)]
15. Zhang, X.-T.; Sato, O.; Taguchi, M.; Einaga, Y.; Murakami, T.; Fujishima, A. Self-Cleaning Particle Coating with Antireflection Properties. *Chem. Mater.* **2005**, *17*, 696–700. [[CrossRef](#)]
16. Ullah, M.; Ban, S.-M.; Kim, D.-S. Optimization of dispersed LaPO₄:Tb nanosol and their photoluminescence properties. *Opt. Mater.* **2019**, *97*, 109366. [[CrossRef](#)]
17. Min, B.H.; Lee, J.C.; Jung, K.Y.; Kim, D.S.; Choi, B.-K.; Kang, W.-J. An aerosol synthesized CeO₂:Eu³⁺/Na⁺ red nanophosphor with enhanced photoluminescence. *RSC Adv.* **2016**, *6*, 81203–81210. [[CrossRef](#)]
18. Jung, K.Y.; Han, J.H.; Kim, D.S.; Choi, B.-K.; Kang, W.-J. Aerosol Synthesis of Gd₂O₃:Eu/Bi Nanophosphor for Preparation of Photofunctional Pearl Pigment as Security Material. *J. Korean Ceram. Soc.* **2018**, *55*, 461–472. [[CrossRef](#)]
19. Lee, S.J.; You, M.S.; Im, S.H. Formation of uniform TiO₂ nanoshell on α -alumina nanoplates for effective metallic luster pigments. *Korean J. Chem. Eng.* **2016**, *33*, 2732–2737. [[CrossRef](#)]
20. Tohidifar, M.; Taheri-Nassaj, E.; Alizadeh, P. Precursor content assessment and its influence on the optical interference of a nano-sized mica-hematite pearlescent pigment. *Powder Technol.* **2010**, *204*, 194–197. [[CrossRef](#)]
21. Lee, H.J.; Ban, S.M.; Jung, K.-Y.; Choi, B.-K.; Kang, K.-J.; Kim, D.S. Nano Dispersion of Aggregated Y₂O₃:Eu Red Phosphor and Photoluminescent Properties of Its Nanosol. *Korean J. Mater. Res.* **2017**, *27*, 100–106. [[CrossRef](#)]
22. Mengual, O.; Meunier, G.; Cayre, I.; Puech, K.; Snabre, P. Characterization of instability of concentrated dispersions by a new optical analyser: The TURBISCAN MA 1000. *Colloids Surfaces A Physicochem. Eng. Asp.* **1999**, 111–123. [[CrossRef](#)]
23. Zuend, A.; Marcolli, C.; Booth, A.M.; Lienhard, D.M.; Soonsin, V.; Krieger, U.K.; Topping, D.O.; McFiggans, G.; Peter, T.; Seinfeld, J.H. New and extended parameterization of the thermodynamic model AIOMFAC: Calculation of activity coefficients for organic-inorganic mixtures containing carboxyl, hydroxyl, carbonyl, ether, ester, alkenyl, alkyl, and aromatic functional groups. *Atmos. Chem. Phys. Discuss.* **2011**, *11*, 9155–9206. [[CrossRef](#)]
24. Gupta, B.K.; Haranath, D.; Saini, S.; Singh, V.N.; Shanker, V. Synthesis and characterization of ultra-fine Y₂O₃:Eu³⁺ nanophosphors for luminescent security ink applications. *Nanotechnology* **2010**, *21*, 055607. [[CrossRef](#)] [[PubMed](#)]
25. Su, C.Y.; Tang, H.Z.; Zhu, G.D.; Li, C.C.; Lin, C.K. The optical properties and sunscreen application of spherical h-BN-TiO₂/mica composite powder. *Ceram. Int.* **2014**, 4691–4696. [[CrossRef](#)]